CoFe-double hydroxide honeycomb covering $CuCo_2O_4$ nanosheets as core-shell nanostructure catalyst for efficient electrocatalytic nitrate conversion to ammonia

Zijuan Zhao‡, Xiujuan Zhang‡, Yinghao Li, Shuxian Qin and Xiaoqiang Liu *

Henan International Joint Laboratory of Medicinal Plants Utilization, College of Chemistry and Molecular Sciences, Henan University, Zhengzhou 450046, China.

‡ These authors contributed equally to this work.

* Corresponding authors.

E-mail addresses: liuxq@henu.edu.cn (X. Liu)

S1. Characterization instruments

X-ray diffraction (XRD) pattern was obtained at a Bruker D8 Advance diffractometer (Bruker, Germany) equipped with Cu Kα radiation. Energy dispersive spectrum (EDS) and scanning electron microscopic (SEM) images were obtained by a Carl Zeiss Gemini SEM 500 scanning electron microscope (Zeiss, Germany) equipped with an energy disperse spectrometer manufactured by Oxford Instrument Corporation. High-

resolution transmission electron microscopic (HRTEM) images were acquired at a FEI Tecnai G20 s-twin 200 kV transmission electron microscope (FEI, America). X-ray photoelectron spectroscopy (XPS) data were obtained at an XPS spectrometer (Thermo scientific K-Alpha, America), equipped with an AI K Alpha radiation source with a test energy of 1486.8 eV and a beam spot of 400 μm. The absorbance data of samples were measured with a UH-4150 UV–vis spectrophotometer (Hitachi, Japan). Nuclear Magnetic Resonance (NMR) test was conducted with Bruker ascend 500 (Bruker，Germany). Attenuated Total Reflectance Fourier Transform Infrared Spectroscopy (ATR-FTIR) was performed at a FTIR-8900 (Bruker，Germany).

S2. Experimental section

S2.1. Materials

Carbon cloth was purchased from Dongguan Kelud Innovation Technology Co., Ltd (China). Potassium nitrate (KNO_3) was purchased from Tianjin Kermel Chemical Reagent Co, Ltd (China). Ethanol (C_2H_6O) and tert-Butanol (TBA) were ordered from Tianjin Fuyu Fine Chemical Co, Ltd (China). Hydrochloric acid (HCl) and nitric acid (HNO_3) were purchased from Luoyang Haohua Chemical Reagent Co., Ltd (China). Mercury iodide (HgI_2) was purchased from Shanghai RON Reagent Co., Ltd (China). Cobaltous nitrate hexahydrate ($Co(NO_3)_2·6H_2O$), urea ($CO(NH_2)_2$), ammonium fluoride (NH_4F), ferrous sulfate ($FeSO_4·7H_2O$), copper nitrate trihydrate ($Cu(NO_3)_2·3H_2O$), sodium sulfate (Na_2SO_4), sulfamic acid (H_3NO_3S), N-(1-naphthyl) ethylenediamine dihydrochloride ($C_{12}H_{14}N_2·2HCl$), sulfonamide ($C_6H_8N_2O_2S$), potassium sodium tartrate tetrahydrate ($C_4H_4O_6KNa·4H_2O$), ammonium chloride

(NH_4Cl) and potassium iodide (KI) were purchased from Shanghai Aladdin Biochemical Technology Co., Ltd (China). All reagents are analytical grade and used without further purification. The ultra-pure water used in all experiments was purified through the Millipore system.

S2.2. Preparation of $CuCo_2O_4$|CC, Co_3O_4|CC and CuO|CC

Initially, 0.291 g $Co(NO_3)_2 \cdot 6H_2O$, 0.121 g $Cu(NO_3)_2 \cdot 3H_2O$, 0.3 g $CO(NH_2)_2$ and 0.1 g NH_4F were dissolved in 35 mL of distilled water and stirred with a magnetic mixer for 30 minutes, before a piece of carbon cloth was dipped into the above mixed solution. The resulting solution, along with the carbon cloth, were then transferred into a 50 mL Teflon-lined stainless-steel reactor and placed in an oven at 120 °C for 6 hours. After the reactor was cooled to room temperature, the carbon cloth was collected, washed with ethanol and distilled water several times, and then dried at 60°C. Finally, the dried material was heated to 350 ℃ in Muffle furnace at a heating rate of 2 ℃ min^{-1} and kept at 350 ℃ for 2 hours to obtain $CuCo_2O_4$|CC. The preparation method of Co_3O_4|CC is similar to that of $CuCo_2O_4$|CC, except that 0.121 g of $Cu(NO_3)_2 \cdot 3H_2O$ was not added in the preparation process. Similarly, the preparation method of CuO|CC is similar to that of $CuCo_2O_4$|CC, except that 0.291 g of $Co(NO_3)_2 \cdot 6H_2O$ was not added in this process.

S2.3. Electrochemical measurements

All electrochemical tests were performed with a three-electrode configuration in a two-compartment cell (100 mL) separated by a proton exchange membrane (Nafion 117) using a Zahner Ennium electrochemical workstation. The proton exchange

membrane was first pre-treated in hydrogen peroxide (5% mass fraction) at 80 ℃ for 1 hour, then soaked in ultra-pure water for 30 minutes, subsequently treated with 5% sulfuric acid at 80 ℃ for 1 hour, and finally soaked in ultra-pure water for 30 minutes. $RuIrO_2$|Ti (5cm×3cm) electrode and Ag|AgCl (filled with saturated KCl solution) electrode are adopted as the counter and reference electrodes, respectively. Carbon cloth, $CuCo_2O_4$|CC, Co_3O_4|CC, CuO|CC, CoFe-LDH@$CuCo_2O_4$|CC and CoFe-LDH|CC are all used as the working electrodes. Moreover, 0.5 M Na_2SO_4 is used as the supporting electrolyte, and the electrode soaking area in both anode chamber and cathode chamber is controlled to ~7 cm^2. All reactions were carried out at room temperature under a magnetic stirring rate of ~300 rpm, and a pH value of 7.10 was retained for all the test solutions. According to the formula of $E_{RHE} = E_{Ag/AgCl} + 0.198 + 0.059 \times pH$, all the measured potentials were converted to RHE relative to the reversible hydrogen electrode. Electrochemically active surface area (ECSA) was evaluated from double-layer capacitance (C_{dl}) according to the following equation:

$$ECSA = C_{dl}/C_s$$

Where C_s is the specific capacitance of smooth surface of the prepared materials under specific electrochemical conditions.

S2.4. Determination method

S2.4.1. Determination of NO_3^--N

First, after the electrochemical test, a certain amount of electrolyte was taken out from the electrolytic cell and diluted to 5 mL with a concentration within the detection range

of the standard curve. Then, 100 μL of 1 M hydrochloric acid (HCl) solution and 10 μL of 0.8 wt% sulfamic acid (H_3NO_3S) solution were added to the diluted sample solution. After being well shaken and kept still for 15 minutes the absorbance of the diluted electrolyte at 220 nm and 275 nm was measured by UV-Vis spectrophotometer. Then, the absorbance at 220 nm was subtracted from that at 275 nm to obtain the true absorbance of NO_3^--N ($A = A_{220nm}$-2 A_{275nm}). At the same time, a series of 5 mL KNO_3 standard solutions (0.25, 0.50, 1.00, 1.50, and 2.00 mg N L^{-1}) were prepared, and respectively mixed with100 μL of 1 M HCl solution and 10 μL of 0.8 wt% H_3NO_3S solution (color developing agent). The absorbance of standard solutions at 220 nm and 275 nm wavelength were measured, and the standard curve (Figure S1) was drawn with the concentrations of NO_3^--N versus the relative absorbance ($A = A_{220nm}$-2 A_{275nm}) to quantitatively calculate the nitrate concentrations in the measured solutions after the electrochemical reduction reactions.

S2.4.2. Determination of NO_2^--N

In this experiment, Griess reagent was used as the color developing agent, and prepared as follows. First, 2 g of p-aminobenzenesulfonamide was dissolved in a mixed solution of 25 mL of ultra-pure water and 5 mL of concentrated phosphoric acid (ρ = 1.70 g mL^{-1}). Then, 0.1 g of naphthalenediamine hydrochloride was added into the above solution and stirred until dissolved. After the electrochemical test, a certain amount of electrolyte was taken from the electrolytic cell and diluted to 5 mL with a concentration within the standard curve detection range. Then, 100 μL of the prepared Griess reagent was added to the diluted sample solution, well shaken and kept still for

15 minutes before the absorbance of the diluted electrolyte at 540 nm was measured by the UV-Vis spectrophotometer. At the same time, a series of 5 mL $NaNO_2$ standard solutions (0.025, 0.050, 0.100, 0.150, 0.200 mg N L^{-1}) were prepared, and equal volume of the Griess reagent was respectively added into the above solutions as the color developer. The absorbance of the standard solutions at 540 nm was measured to draw a concentration versus absorbance standard curve (Figure S2), which can be used to quantitatively calculate the concentration of nitrite in the measured solution after the electrochemical reduction reaction.

S2.4.3. Determination of NH_3-N

In this experiment, Nessler reagent was used as the color developing agent and prepared as follows. First, 8.0 g of sodium hydroxide was dissolved in 25 mL of ultra-pure water to obtain solution I. Secondly, 3.5 g of potassium iodide and 5.0 g of mercury iodide were dissolved in 25 mL of ultra-pure water to obtain solution II. The Nessler reagent was obtained by gradually adding the above solution II to solution I and stirring the mixed solution vigorously. After remaining still for 24 hours, the supernatant of Nessler reagent was collected for the subsequent ammonia detection. Meanwhile, the ammonia detection process also requires $C_4H_4O_6KNa{\cdot}4H_2O$ solution (ρ = 500 g/L), which was prepared as follows. Firstly, 25.0 g of $KNaC_4H_6O_6{\cdot}4H_2O$ was dissolved in 50 mL ultra-pure water and heated till boiling to remove the ammonium residue. Afterwards, the boiling solution was cooled to ambient temperature and then diluted to 100 mL. After the electrochemical test, a certain amount of electrolyte was taken out from the electrolytic cell and diluted to a 5 mL solution with a concentration within the

standard curve detection range. Then, 100 μL of $C_4H_4O_6KNa{\cdot}4H_2O$ solution (ρ = 500 g/L) was added into the electrolyte solution to reduce the interference from other metal ions, and then 100 μL Nessler reagent was added to the above solution for color development. After the test solution was well shaken and remained still for 15 minutes, the absorbance at 420 nm was measured by UV-Vis spectrophotometry. Meanwhile, a series of 5 mL NH_4Cl standard solutions (0.025, 0.050, 0.100, 0.150, 0.200 mg N L^{-1}) were prepared and mixed with 100 μL $C_4H_4O_6KNa{\cdot}4H_2O$ solution (ρ = 500 g/L) and 100 μL Nessler reagent. The absorbance of standard solutions at 420 nm was measured, and the standard curve (Figure S3) was plotted using the concentration versus measured absorbance to quantitatively calculate the ammonia concentration in the test solutions after the electrochemical reduction reaction.

S2.5. Calculation equations

In this work, conversion percentage of NO_3^-, NO_2^- selectivity, NH_3 selectivity, NH_3 Faraday efficiency (FE), ammonia NH_3-N yield rate were calculated according to the following formulas:

$$Conversion\ percentage\ of\ NO_3^- = \Delta[NO_3^- - N]/[NO_3^- - N]_0 \times 100\%$$

$$NO_2^-\ selectivity = \Delta[NO_2^- - N]/\Delta[NO_3^- - N] \times 100\%$$

$$NH_3\ selectivity = \Delta[NH_3 - N]/\Delta[NO_3^- - N] \times 100\%$$

$$FE = F \times \Delta[NH_3 - N] \times V \times 8/(M_N \times Q) \times 100\%$$

$$[NH_3 - N]\ yield\ rate = (\Delta[NH_3 - N] \times V)/(M_N \times S \times t)$$

Also, a pseudo-first-order kinetic fitting model was used to describe the relationship between NO_3^--N concentration and electrocatalytic time, as shown below:

$[NO_3^- - N]_t/[NO_3^- - N]_0 = exp(-kt)$

Herein, $\Delta[NO_3^- - N]$ represents the concentration difference of $NO_3^- - N$ after the electrocatalytic reaction; $[NO_3^- - N]_0$ indicates the initial concentration of $NO_3^- - N$; $\Delta[NO_2^- - N]$ represents the difference between the concentration at reaction time t and the initial concentration; $\Delta[NH_3 - N]$ is the concentration difference of $NH_3 - N$ after the electrocatalytic reaction; F is Faraday's constant (96500 C mol^{-1}); V represents the volume of electrolyte solution in the electrolytic cell; M_N is the molar mass of N (14 g mol^{-1}); Q is the total amount of electric charge passing through the electrode during the whole reaction process; S represents the geometric area (7 cm^2) of the working electrode immersed in the electrolyte; and t represents the electrocatalytic reaction time.

Turnover frequency (TOF) of the catalyst materials was calculated according to

$TOF = \Delta n(\mu g\ cm^{-2}\ h^{-1})/ECSA$

Where $\Delta n(\mu g\ cm^{-2}\ h^{-1})$ is the $NH_3 - N$ yield rate per geometry unit area (cm^2) of the catalyst on CC per unit time (hour).

S2.6. Density functional theory calculation

Theoretical validation of the CoFe-LDH@$CuCo_2O_4$|CC heterojunction was carried out through modeling in Materials Studio software. In the modeling of CoFe-LDH@$CuCo_2O_4$|CC, the lattice matching ratio between CoFe-LDH and $CuCo_2O_4$ remains at approximately 5%, which helps maintain interfacial structural stability and performance, effectively reducing interfacial defects and stress accumulation. This meets the stringent requirements for theoretical modeling and

subsequent calculations, thereby providing a fundamental basis for the accurate construction of the CoFe-LDH@$CuCo_2O_4$|CC heterojunction. The DFT computational models of individual $CuCo_2O_4$, CoFe-LDH and the CoFe-LDH@$CuCo_2O_4$ composite were constructed for comparison purpose. Specifically, we constructed the three models with a 15-angstrom vacuum layer to avoid inter-layer interactions. Additionally, the Grimme (DFT-D3) method was used to correct weak van der Waals interactions. For the convergence of the ion steps in the calculation, the upper limit of plane wave basis energy, force convergence threshold and total energy was set at 500 eV, 0.02 eV $Å^{-1}$, and less than 10^{-5} eV, respectively. The VASPKIT software was used to establish a k-point Gamma network with an interval of 0.04 $Å^{-1}$ for static self-consistent calculations.

All calculations in this study were performed using the Vienna ab initio simulation package (VASP) based on the density functional theory (DFT). The projected augmented wave (PAW) was employed for the generation of the pseudopotential with a cutoff energy of 450 eV. The Brillouin zone was sampled by a 3 × 4 × 1 special k-point. The force convergence threshold was 0.02 eV $Å^{-1}$ and the total energy was less than 10^{-5} eV. To calculate the free energy change during the nitrite reduction process, the computational hydrogen electrode (CHE) model was used as follows:

$$\Delta G = \Delta E_{DFT} + \Delta E_{ZPE} - T\Delta S + eU + \Delta G_{pH}$$

where ΔE_{DFT} is the eletronic energy difference from direct DFT calculation, ΔE_{ZPE} is the contribution of the vibration energy of intermediates adsorbed on the catalyst surface. $T\Delta S$ is the entropic contribution, and T was set as 298K throughout the

calculation. U is the applied potential and ΔG_{pH} is the modification originating from of pH. The last two terms were omitted because U and pH were assumed to be constant in this work.

The adsorption energy (E_{ad}) on all the catalyst structures can be calculated by:

$$E_{ad} = E_{total}l - E_{heterojunction} - E_{NO_3}$$

Where E_{total}, $E_{heterojunction}$ and E_{NO_3} respectively represent the adsorption total structure and heterojunction energy, as well as the nitrate energy.

To calculate the Charge Density Difference (CDD), the following formula is used:

$$CDD = \rho_{heterojunction} - \rho_{CuCo_2O_4} - \rho_{CoFe-LDH}$$

Herein, $\rho_{CuCo_2O_4}$, $\rho_{CoFe-LDH}$ and $\rho_{heterojunction}$ is charge density for $CuCo_2O_4$|CC, CoFe-LDH|CC, and CoFe-LDH@$CuCo_2O_4$|CC.

S2.7. In situ ATR-FTIR

In situ attenuated total reflection Fourier transform infrared (ATR-FTIR) spectra were acquired using an infrared spectrometer (FTIR-8900, Bruker) equipped with a liquid nitrogen-cooled mercury cadmium telluride (MCT) detector. Initially, CoFe-LDH@$CuCo_2O_4$ was scraped from CoFe-LDH@$CuCo_2O_4$|carbon cloth (CC) and dispersed into a suspension. Subsequently, the suspension was drop-cast onto a home-made gold-coated silicon prism, which served as the working electrode. A platinum electrode and an Ag|AgCl electrode (saturated with KCl) were employed as the counter electrode and reference electrode, respectively. During the measurements, the infrared beam was incident at a 60° angle through the prism, reaching the interface between the CoFe-LDH@$CuCo_2O_4$ catalyst and the electrolyte, and the reflected beam was

collected by the MCT detector. The electrocatalytic tests were performed within an applied potential window of -0.1 to -0.5 V (vs. RHE) versus the reversible hydrogen electrode, and the background spectrum was recorded at the open-circuit potential (OCP).

S3. Figures

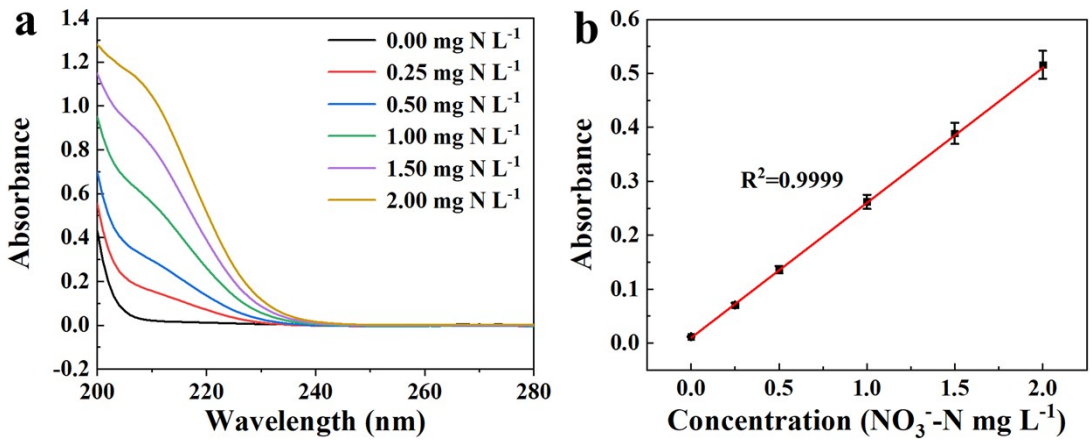

Figure S1. (a) UV-Vis spectra of standard NO_3^--N solutions with different concentrations; (b) Calibration plot constructed with UV-Vis absorption of NO_3^--N standard solutions at 220 nm versus NO_3^--N concentrations.

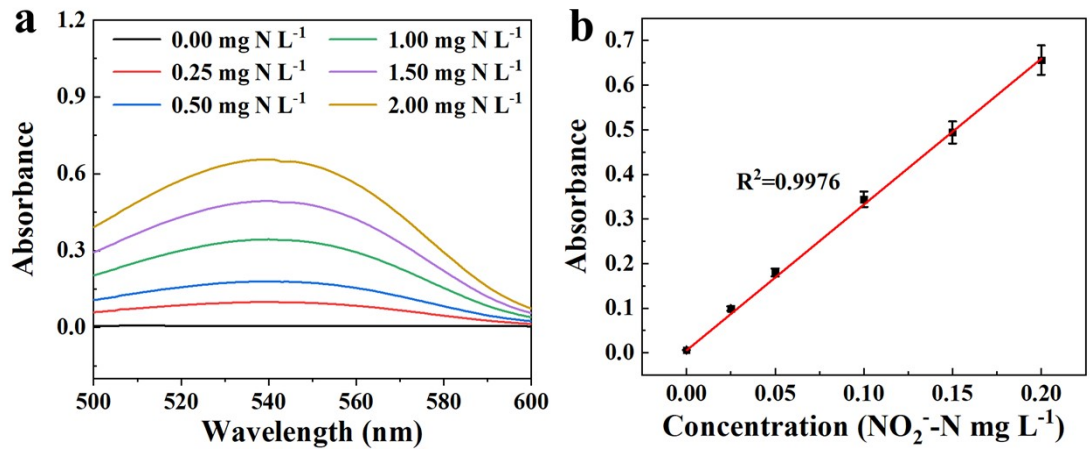

Figure S2. (a) UV-Vis spectra of standard NO_2^--N solutions with different concentrations; (b) Calibration plot constructed with UV-Vis absorption of NO_2^--N standard solutions at 540 nm versus NO_2^--N concentrations.

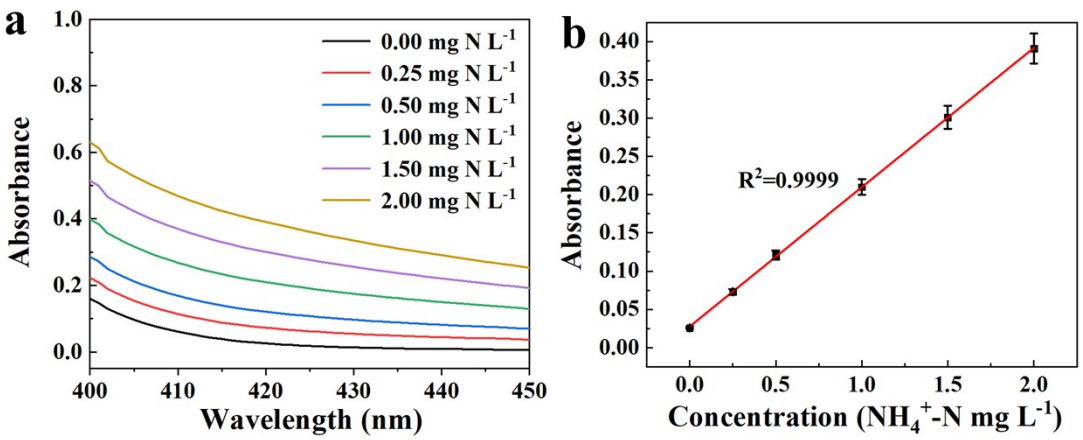

Figure S3. (a) UV-Vis spectra of standard NH_3-N solutions with different concentrations; (b) Calibration plot constructed with UV-Vis absorption of NH_3-N standard solutions at 420 nm versus NH_3-N concentrations.

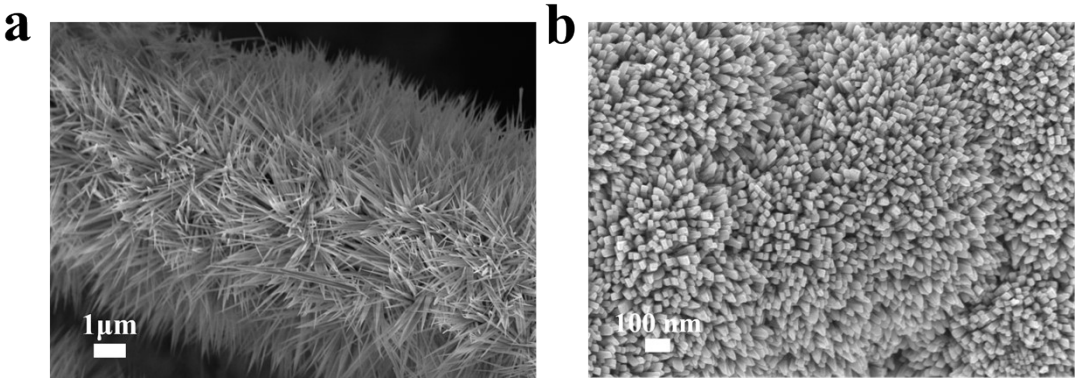

Figure S4. (a) SEM images of Co_3O_4|CC and (b) CuO|CC.

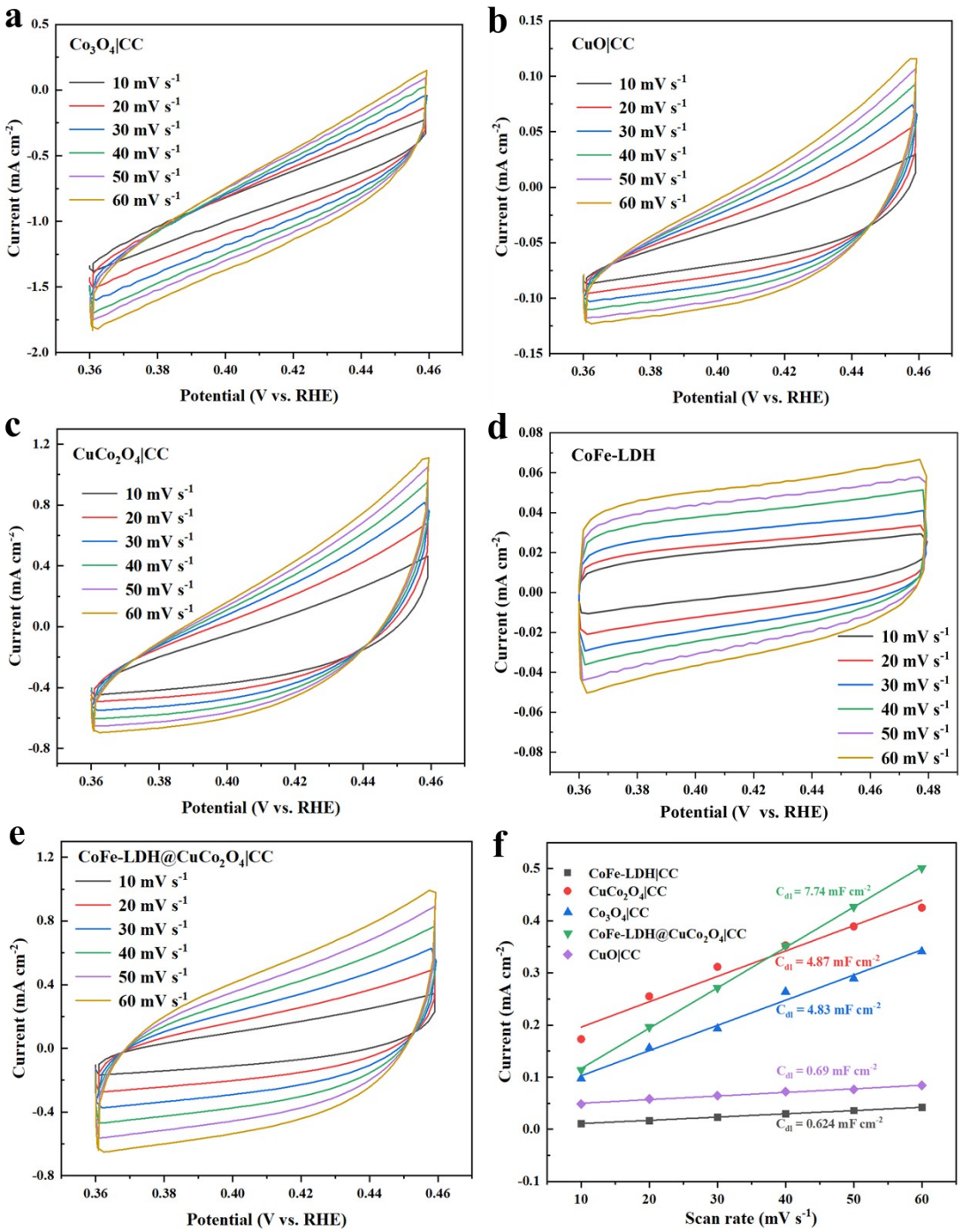

Figure S5. Cyclic voltammetry curves of (a) Co_3O_4|CC; (b) CuO|CC; (c) $CuCo_2O_4$|CC; (d) CoFe-LDH|CC; and (e) CoFe-LDH@$CuCo_2O_4$|CC at scan rates ranging from 10 mV s^{-1}-60 mV s^{-1}; (f) C_{dl} values of different catalysts obtained from above cyclic voltammograms.

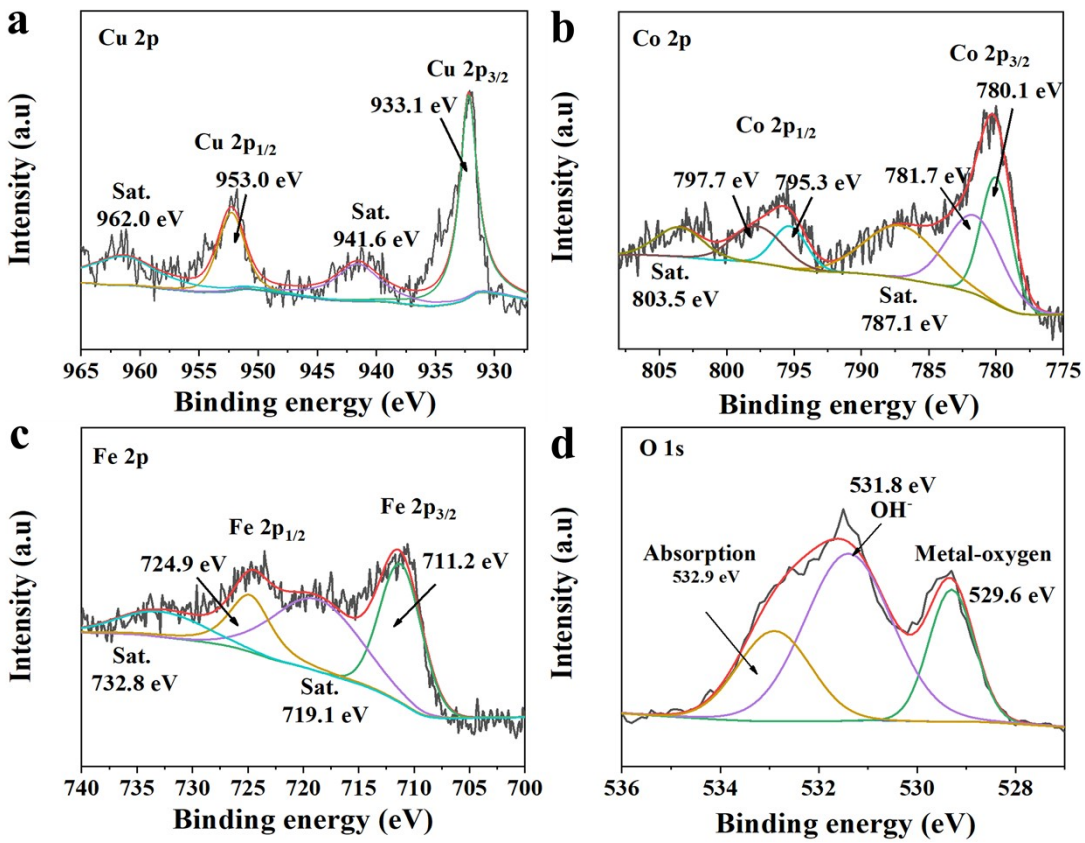

Figure S6. High-resolution XPS spectra of Cu, Co, Fe and O in CoFe-LDH@$CuCo_2O_4$|CC after 14 cycles of stability tests.

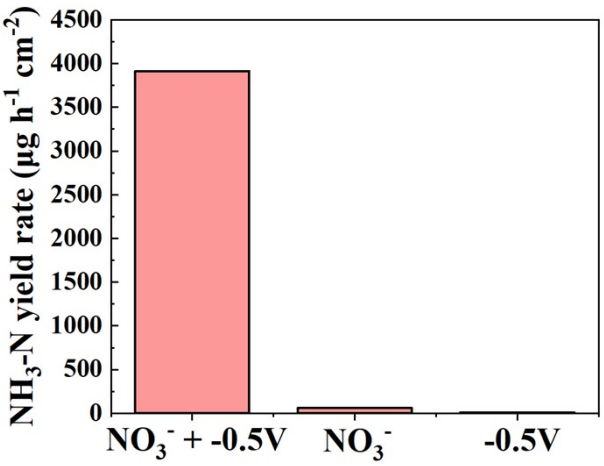

Figure S7. Ammonia yields under three different conditions.

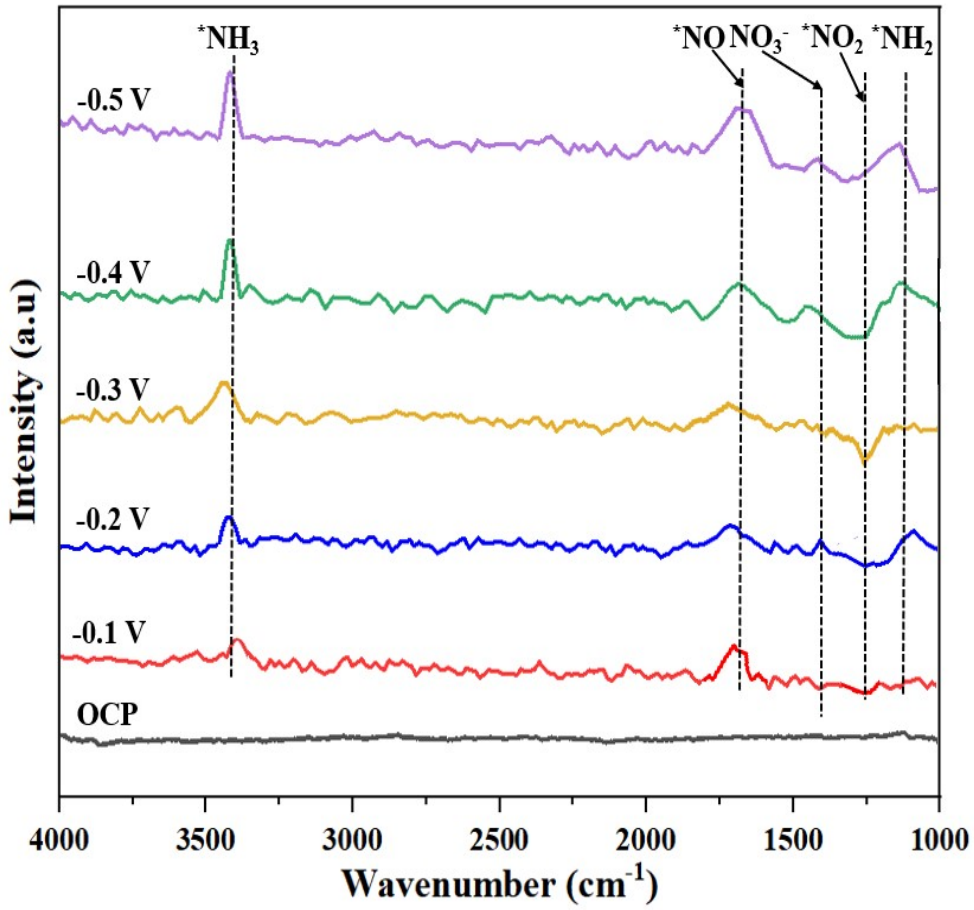

Figure S8. ATR-FTIR of test solutions containing 400 ppm NO_3^--N and 0.5 M Na_2SO_4 at different potentials on CoFe-LDH@$CuCo_2O_4$.

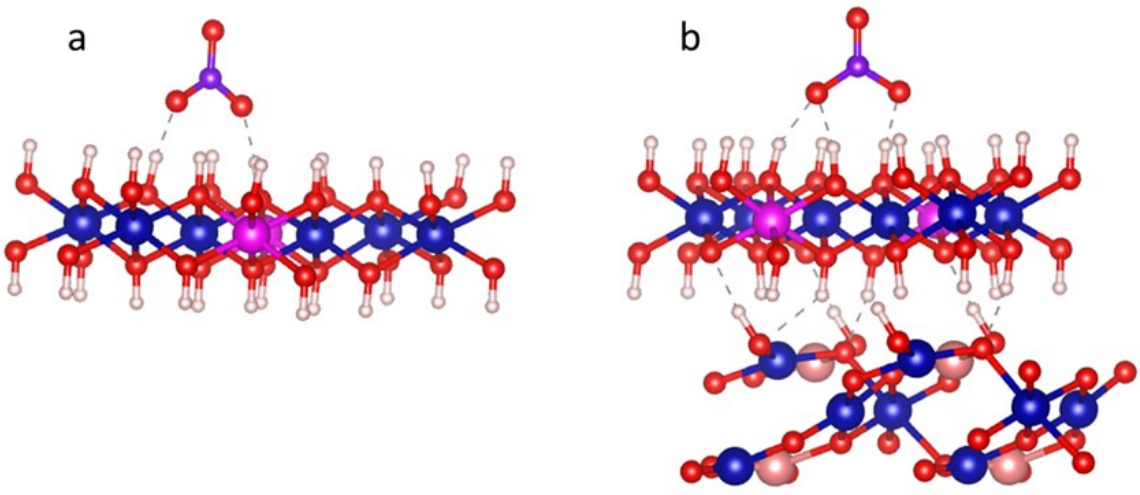

Figure S9. Adsorption configurations of NO_3^- on(a)CoFe-LDH, (b) CoFe-LDH@$CuCo_2O_4$.

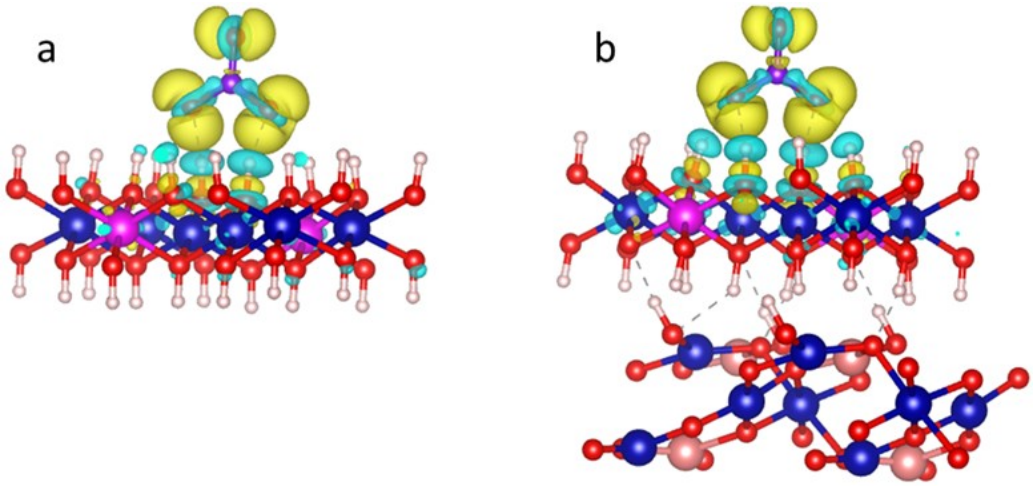

Figure S10. Charge Density Difference of NO_3^- adsorbed on (a)CoFe LDH, (b) CoFe-LDH@$CuCo_2O_4$.

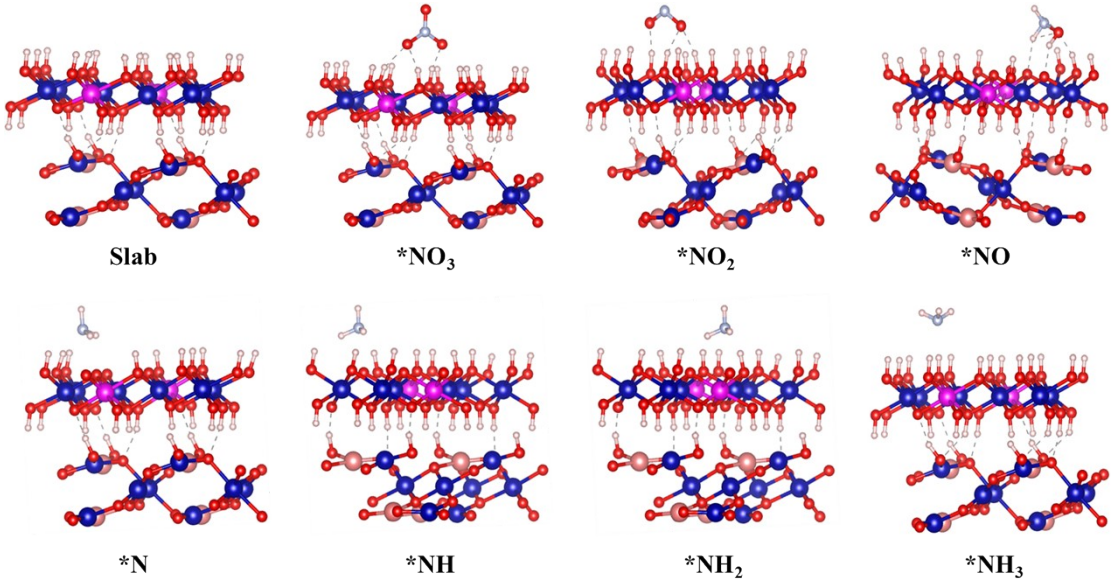

Figure S11. Adsorption configurations of reaction intermediates on CoFe-LDH@$CuCo_2O_4$ surface during ECNO_3R. Red, white, purple, blue, pink and orange balls represent O, H, N, Co, Fe and Cu atoms, respectively.

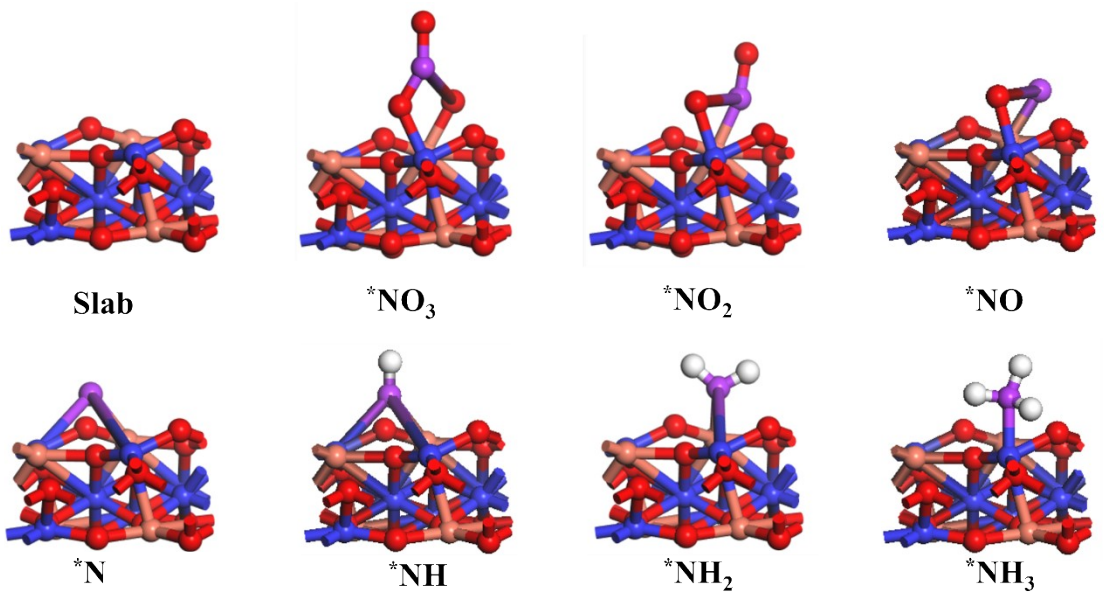

Figure S12. Adsorption configurations of reaction intermediates on $CuCo_2O_4$ surface during $ECNO_3R$. Red, white, purple, blue and orange balls represent O, H, N, Co and Cu atoms, respectively.

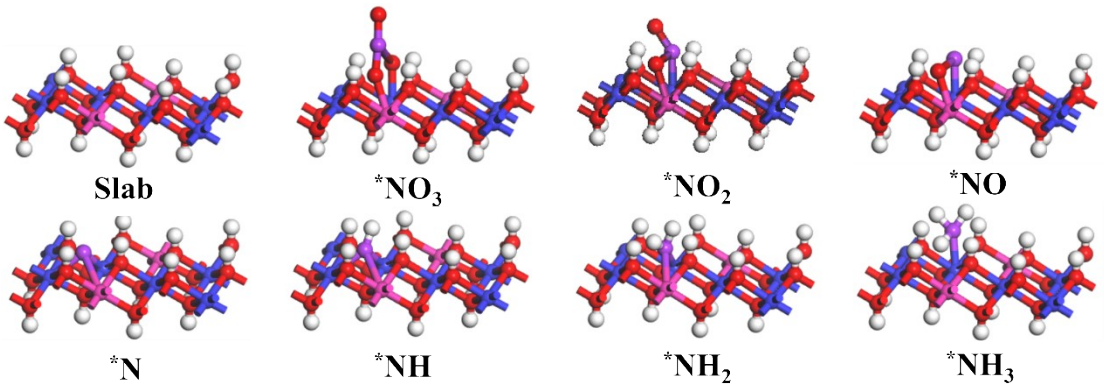

Figure S13. Adsorption configurations of reaction intermediates on CoFe-LDH surface during $ECNO_3R$. Red, white, purple, blue and pink balls represent O, H, N, Co and Fe atoms, respectively.

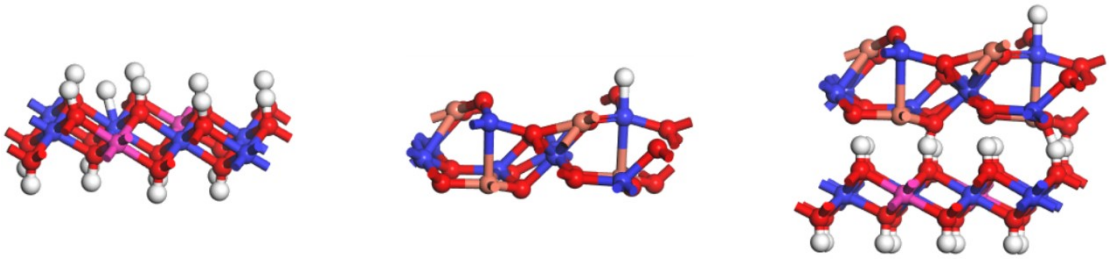

Figure S14. Adsorption configurations of atomic *H on CoFe-LDH, $CuCo_2O_4$ and $CuCo_2O_4$@CoFe-LDH. Red, white, purple, blue, pink and orange balls represent O, H, N, Co, Fe and Cu atoms, respectively.

Table S1. Performance comparison between recently reported ECNO$_3$R electrocatalysts at ambient conditions.

Catalyst	Electrolyte	Potential (V Vs.RHE)	NH_3 selectivity (%)	FE(%)	Ref.
CoFe-LDH@$CuCo_2O_4$|CC	0.5 M Na_2SO_4 (400 ppm NO_3^--N)	-0.4	91.1	91.2	This work
CuCo/MCS	0.1 m Na_2SO_4 (50 mg L^{-1} NO_3^-–N)	-0.58	91.2	94	1
CuCo-NC	0.2 M K_2SO_4 (5 mM NO_3^-)	-0.74	80	77	2
Cu2O/Co3O4@NC	1.0 M KOH (0.1 M KNO_3)	-0.45	87.38	96.75	3
Fe-F-NiO NNAs	0.1 M K_2SO_4 (0.1 M KNO_3)	−1.198	82.5	82.5	4
TiO_2 NTs	0.5 M K_2SO_4 (0.49 mM KNO_3)	−0.948	87.1	85	5

1. Xue, Y., J. Bian, Y. Jia, H. Wang, T. Wang, M. Li, R. Liu, H. Liu and J. Qu,Enzyme-Mimicking Confined Cu–Co Dual Sites for Selective Electrocatalytic Reduction of Dilute Nitrate to Ammonia, *Advanced Functional Materials*, 2025.
2. Shu, S., Y. Chen, H. Xiang and Y. Chu,Selective Electroreduction of Nitrates to Ammonia by

Enhanced Byproduct Conversion over a Tandem CuCo-NC Catalyst, *Industrial & Engineering Chemistry Research*, 2025, **64**, 4342-4352.

3. Dai, L. Z., G. Y. Yong, W. N. Gan, T. Li, Z. C. Chen, L. Y. Pan, H. Q. Luo and N. B. Li,Self-reconstructed Cu2O/Co3O4@NC heterostructured catalyst for efficient tandem electrocatalytic conversion of nitrate to ammonia, *Chemical Engineering Journal*, 2025, **521**.
4. Bilal, A., A. Bahadur, S. Iqbal, S. Mahmood, I. Khan, I. M. Khan, M. Sajjad, S. Ali, N. M. Musyoka, G. Liu, A.-E. Farouk and N. M. Alyami,Innovative Fe-F-Co-doped NiO nanoarrays: Pioneering high-efficiency electrochemical nitrate reduction to ammonia, *Journal of Environmental Chemical Engineering*, 2025, **13**.
5. Jia, R., Y. Wang, C. Wang, Y. Ling, Y. Yu and B. Zhang,Boosting Selective Nitrate Electroreduction to Ammonium by Constructing Oxygen Vacancies in TiO2, *ACS Catalysis*, 2020, **10**, 3533-3540.